Molecules and Cells

Experimental Applications of *in situ* Liver Perfusion Machinery for the Study of Liver Disease

Won-Mook Choi[1], Hyuk Soo Eun[2], Young-Sun Lee[3], Sun Jun Kim[2], Myung-Ho Kim[1], Jun-Hee Lee[1], Young-Ri Shim[1], Hee-Hoon Kim[1], Ye Eun Kim[1], Hyon-Seung Yi[1,2,*], and Won-Il Jeong[1,*]

[1]Laboratory of Liver Research, Graduate School of Medical Science and Engineering, KAIST, Daejeon, Korea, [2]Department of Internal Medicine, Chungnam National University School of Medicine, Daejeon, Korea, [3]Department of Internal Medicine, Korea University College of Medicine, Korea
*Correspondence: jmpbooks@cnuh.co.kr (HSY); wijeong@kaist.ac.kr (WIJ)
http://dx.doi.org/10.14348/molcells.2018.0330
www.molcells.org

The liver is involved in a wide range of activities in vertebrates and some other animals, including metabolism, protein synthesis, detoxification, and the immune system. Until now, various methods have been devised to study liver diseases; however, each method has its own limitations. *In situ* liver perfusion machinery, originally developed in rats, has been successfully adapted to mice, enabling the study of liver diseases. Here we describe the protocol, which is a simple but widely applicable method for investigating the liver diseases. The liver is perfused *in situ* by cannulation of the portal vein and suprahepatic inferior vena cava (IVC), with antegrade closed circuit circulation completed by clamping the infrahepatic IVC. *In situ* liver perfusion can be utilized to evaluate immune cell migration and function, hemodynamics and related cellular reactions in each type of hepatic cells, and the metabolism of toxic or other compounds by changing the composition of the circulating media. *In situ* liver perfusion method maintains liver function and cell viability for up to 2 h. This study also describes an optional protocol using density-gradient centrifugation for the separation of different types of hepatic cells, allowing the determination of changes in each cell type. In summary, this method of *in situ* liver perfusion will be useful for studying liver diseases as a complement to other established methods.

Keywords: hemodynamics, immune cell, *in situ* perfusion, liver disease, metabolism

INTRODUCTION

The liver is a pivotal organ in metabolism, coordinating whole-body energy balance by regulating glucose, lipid, and protein metabolism. Moreover, the liver plays a critical role in detoxification, eliminating various toxins and metabolizing drugs and xenobiotics. Following the isolation of rat (Berry and Friend, 1969; Seglen, 1976) and human (Bojar et al., 1976) primary hepatocytes, methods involving isolated primary hepatocytes cultured *in vitro* have been regarded as a gold standard for research on the liver. However, the complex intercellular interactions of the various cell types present in the liver have raised fundamental questions about this methodology.

About 60% of liver cells are hepatocytes, with the other 40% including hepatic stellate cells (HSCs), Kupffer cells (KCs), liver sinusoidal endothelial cells (LSECs), cholangiocytes, and various immune system cells infiltrating the liver (Blouin et al., 1977). Moreover, the liver has significant immunological properties (Gao et al., 2008). Thus, a model

Received 2 August 2018; revised 29 September 2018; accepted 18 October 2018; published online 12 December, 2018

eISSN: 0219-1032

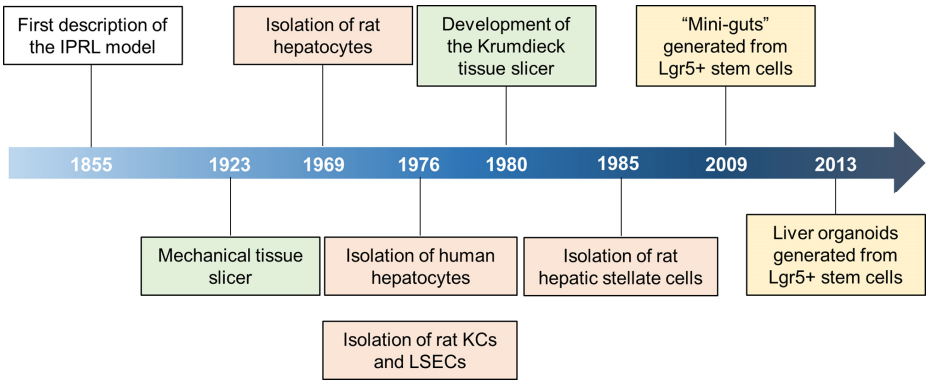

Fig. 1. Timeline showing the development of methods for liver research.

that includes all cell types in their natural environment is required to understand the physiology and pathophysiology of the liver. This understanding would be enhanced by examining the intracellular reactions that take place in each cell type after experimental manipulation. Various methods have therefore been devised and widely applied to study liver disease, including the precision-cut liver slice model and the organoid model, some of which are also applicable to human samples.

Figure 1 briefly depicts the timeline of culture method development in liver research. These methods, however, have limitations, such as the exaggeration of metabolic signaling pathways, the lack of natural matrix implementation, the absence of cell-to-cell interactions (especially with immune cells), and discontinuous hemodynamic considerations in capturing "real-world" phenomena. This study describes a simple method, called *in situ* liver perfusion machinery, which can be adapted to study various liver diseases. This method has been utilized in various murine models of liver diseases (Kim et al., 2017; Lee et al., 2015; 2016; Seo et al., 2016).

MATERIALS AND METHODS

Mice

All animal protocols were approved by the International Animal Care and Use Committee of Korea Advanced Institute of Science and Technology (KAIST, Korea) and conducted in accordance with relevant guidelines and regulations. The mice were maintained on a regular 12-hour light/12-hour dark cycle in a specific pathogen-free animal facility at KAIST. Male mice aged between 8 to 12 weeks were used in the experiments.

In situ liver perfusion

The perfusion system was designed as a closed circuit with a roller pump to provide a constant flow rate (for overview see Fig. 2). First, the portal vein was cannulated, which was the most critical step of the method. It was important to prewarm the water bath and/or the connecting lines to 37℃ before the perfusion. Although puncturing the portal vein of mice may be technically difficult, *in situ* liver perfusion should be circulated through the portal vein to mimic physiologic antegrade circulation. After the portal vein was successfully cannulated (Fig. 2A), the perfusion setup, including the connecting lines and the roller pump, was stabilized by fixation to avoid dislocation of the catheter during circulation. The pump was started to circulate phosphate buffered saline (PBS) solution, resulting in conspicuous distension of the inferior vena cava (IVC) and making the latter easy to cut. After confirming successful cannulation by observing the swelling and discoloration of the liver, the chest was opened to expose the right atrium of the heart (Fig. 2B). The suprahepatic IVC was cannulated through the puncture of the right atrium, with clamping of the infrahepatic IVC causing the solution to exit through the suprahepatic IVC catheter. The system was perfused for 5 min with PBS to flush out blood and prevent clotting of the hepatic vessels (Fig. 2C). The inlet of the line connected to the portal vein was inserted into experimental medium, based on either DMEM (Welgene) or RPMI-1640 (Welgene) supplemented with 10% fetal bovine serum (FBS; Welgene) and 1% penicillin-streptomycin (Gibco). The inlet of the other line connected to the pump was connected to the suprahepatic IVC catheter to close the circuit (Fig. 2D). The lines connected to the portal vein and the suprahepatic IVC should be identical; otherwise, the flow rate of both lines would be different, which may cause the perfused liver to swell or shrink. Alternatively, a 1 ml syringe body can be connected to a suprahepatic IVC catheter to create a flow reservoir. After establishing the closed circuit, circulation can be maintained for up to 2 h with media containing various experimental conditions. The choice of circulating medium and its constituents depended on the aim of the experiment. A minimum of 25 ml of medium was required to establish the closed circuit based on our system with the roller pump (Watson-Marlow) and the connecting lines (cat. no. 14-190-516, Fisher scientific). However, the optimal volume of perfusion medium should be individualized based on each laboratory's own perfusion system. Circulation for more than 2 h is not recommended, because cell viability and function decrease noticeably after 2 h probably due to increased hypoxic stress (Supplementary Fig. S1).

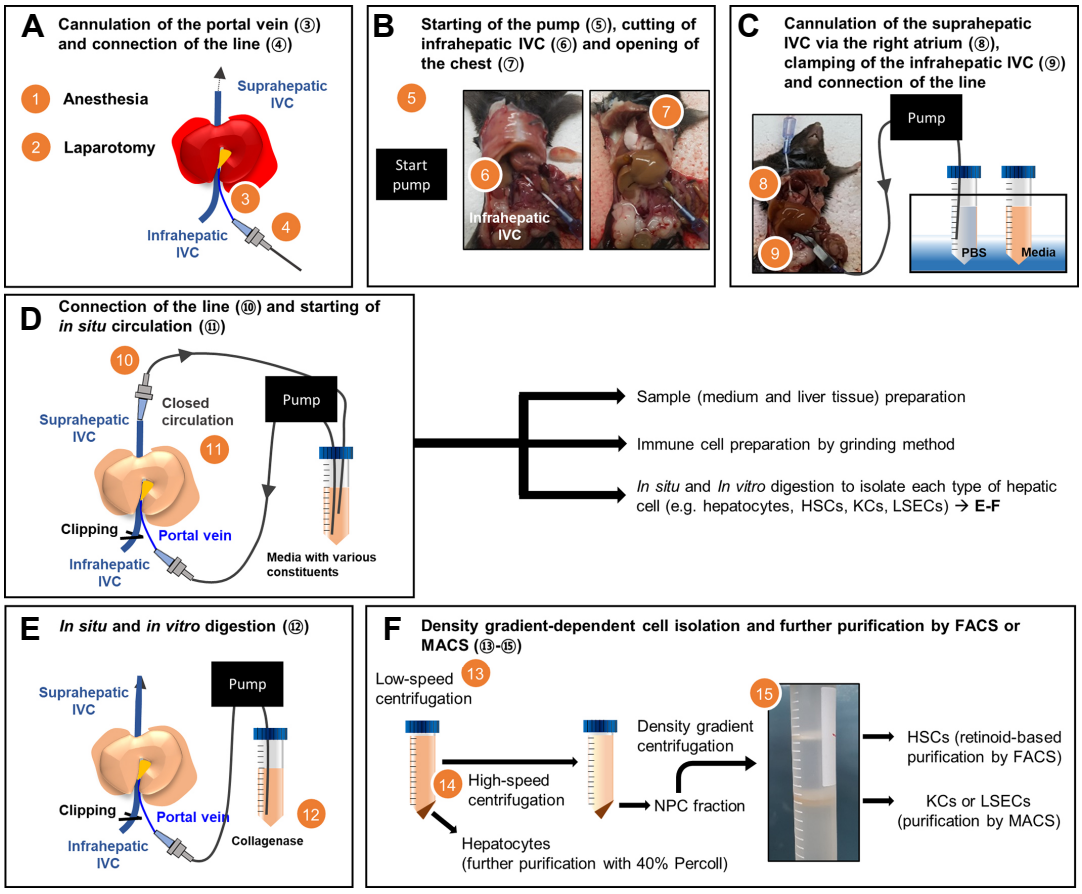

Fig. 2. Overview of the *in situ* hepatic circulation procedure. (A) The anesthetized mouse is cannulated via the portal vein and the line is connected. (B) The pump is started, the infrahepatic inferior vena cava (IVC) is cut off, and the chest of the mouse is opened. (C) The supraheptic IVC is cannulated via the right atrium and the infrahepatic IVC is clamped. The liver is perfused with PBS to eliminate blood. (D) The line is connected to the suprahepatic IVC catheter, followed by closed circulation for up to 2 h. The resulting liver samples can be ground to isolate hepatic immune cells, or further digested with collagenase to isolate each hepatic cell type (e.g. hepatocytes, hepatic stellate cells (HSCs), Kupffer cells (KCs), and liver sinusoidal endothelial cells (LSECs)). (E) Perfusion of the liver with collagenase solution, followed by *in vitro* digestion and filtering of the cell suspension through a 70-μM mesh. (F) Pelleting of hepatocytes by low-speed centrifugation (50×g for 5 min at RT, twice). Hepatocytes can be further purified by 40% Percoll-gradient centrifugation (1,000×g for 10 min at 4℃). Supernatants containing non-parenchymal cells are pelleted by high-speed centrifugation (590×g for 10 min at 4℃, twice) and further separated by density gradient centrifugation (1,600×g for 17 min at 4℃). HSCs can be further purified by retinoid-based FACS sorting. KCs and LSECs can be further purified using F4/80+ and CD146+ MicroBeads, respectively, followed by MACS.

Sample preparation

After the completion of circulation, tissue samples were prepared by 1) using whole liver tissues, 2) grinding liver tissues to isolate hepatic immune cells, or 3) subsequently perfusing the liver tissue with collagenase, followed by density gradient-based separation of hepatic cell types (i.e. hepatocytes, HSCs, KCs, and LSECs) (Figs. 2E and 2F). Briefly, 1) whole liver tissue was cut into small pieces and stored at -80℃ for future analyses such as western blot and qRT-PCR. 2) To isolate hepatic immune cells, mouse livers were ground and passed through a 70-μm cell strainer. The cell suspension was suspended in PBS and centrifuged at 50×g for 5 min to remove hepatocytes. The supernatant was collected, washed with PBS, suspended in 40% Percoll (Merck) in PBS, and centrifuged at 1,000×g for 30 min at 4℃. The cell pellets were resuspended in red blood cell lysis buffer, incubated at 4℃ for 5 minutes, washed with PBS, and centrifuged at 650×g for 15 min at 4℃ to obtain immune cells. 3) For analysis of each hepatic cell (i.e. hepatocytes, HSCs, KCs, and LSECs), subsequent perfusion with collagenase and density gradient-based separation was performed as described, with some modifications (Mederacke et al., 2015; Werner et al., 2015). After removing the line connected to the suprahepatic IVC catheter, the inlet of the line connected to the portal vein was transferred to the collagenase solution of 0.075% collagenase type I and 0.02% DNase I in HBSS buffer, followed by perfusion with this solution for 10 min to digest liver tissues (Fig. 2E). The liver was then carefully extracted

and placed in digestion solution (0.009% collagenase type I and 0.02% DNase I in HBSS). The liver was minced under sterile conditions, placed in digestion solution, and incubated for 20 min at 37℃ with shaking at 90 rpm. The cell suspension was filtered through a 70-μm cell strainer to eliminate any undigested tissue remnants. Primary hepatocytes were separated from non-parenchymal cells (NPCs) by low-speed centrifugation and further purified by 40% Percoll density-gradient centrifugation. NPCs in the supernatant were pelleted by high-speed centrifugation, resuspended in 6 ml density gradient solution (20% Optiprep), followed by sequential layering of 4 ml 11.5% Optiprep solution and 4 ml HBSS and high-speed centrifugation without braking. HSCs were located at the interface between the HBSS and 11.5% Optiprep layers and KCs and LSECs were located in the interface between the 11.5% and 20% Optiprep layers. LSECs were further purified by MACS with CD146+ MicroBeads according to the manufacturer's recommendations. When required, HSCs were further purified by FACS sorting with a 405-nm laser for excitation and a 450/50-nm band-pass filter for detection; and KCs were further purified by FACS or MACS with F4/80+ MicroBeads. Isolated and purified HSCs, KCs, and LSECs were cultured or stored at -80℃ for future analysis.

Histological analyses

Formalin-fixed paraffin-embedded liver sections were stained with hematoxylin and eosin (H&E) using standard protocols. For cytochrome P450 2E1 (CYP2E1) immunohistochemistry, paraffin-embedded tissue sections were incubated with 0.03% H_2O_2 for 30 min to block endogenous peroxidases, followed by incubation with 2.5% normal horse serum for 1 h to block non-specific binding. The tissue samples were incubated with primary antibody to CYP2E1 (Merck) for 30 min at room temperature, followed by incubation with the ImmPRESS HRP Anti-Rabbit IgG Polymer Detection Kit (Vector Laboratories) according to the manufacturer's instructions. Reactions were developed with DAB peroxidase substrate (Vector Laboratories) according to the manufacturer's instructions. The histological features of the tissue samples were monitored and imaged by light microscopy (Olympus).

TUNEL staining

Apoptotic cells were detected using the *in situ* Cell Death Detection Kit (Roche) according to the manufacturer's instructions. Briefly, deparaffinized liver sections were pretreated with proteinase K (Sigma-Aldrich) and incubated with TdT reaction solution in a humidified chamber for 2 h. Positive cells were stained with FITC-avidin D and counterstained with DAPI.

qPCR and western blot analyses

Total RNA was isolated from liver tissues or cells with TRIzol reagent (Thermo Fisher Scientific) and reverse-transcribed to cDNA using amfiRevert II cDNA Synthesis Master Mix (GenDEPOT) or ReverTra Ace® qPCR RT Master Mix with gDNA Remover (Toyobo, Japan) according to the manufacturer's instructions. qPCR was performed using SYBR Green Realtime PCR Master Mix (Toyobo), with the mRNA levels of target genes normalized to the level of *Actb* mRNA in the same sample. The primer pairs used in this study are listed in Supplementary Table S1.

For western blot analyses, total protein samples were isolated from frozen liver tissue or isolated cells using RIPA lysis buffer (30mM Tris, pH 7.5, 150 mM NaCl, 1 mM PMSF, 1 mM Na3VO4, 10% SDS, 10% glycerol), containing a protease and phosphatase inhibitor cocktail (Thermo Fisher Scientific). Samples were separated by 10% SDS-polyacrylamide gel electrophoresis and transferred to nitrocellulose membranes (Thermo Fisher Scientific). After incubating the membranes with 5% skim milk or 5% BSA for 1 h at room temperature to block non-specific binding, the membranes were incubated with primary antibodies overnight at 4℃ and then with the corresponding secondary antibodies for 1 h at room temperature. All of the primary antibodies were diluted 1:1000. Primary antibodies to CYP2E1 and β-actin were purchased from Merck and Sigma-Aldrich, respectively, whereas primary antibodies to other proteins such as HIF-1α, cleaved caspase 3, pSTAT1, STAT1, pJNK, JNK, peNOS, and eNOS were from Cell Signaling Technology. Secondary antibodies used for western blot analyses were HRP-linked anti-rabbit IgG (Cell Signaling Technology) and HRP-linked anti-mouse IgG (H+L) (Thermo Fisher Scientific), both diluted 1:2000. Immunoreactive bands were detected using the ECL detection system with a PhosphorImager (GE Healthcare). Protein expression levels were normalized to the levels in the same samples of β-actin, which was used as a loading control.

Clinical chemistry measurements

Liver injury was evaluated by measuring alanine aminotransferase (ALT) in the perfusate (circulated media) using a VetTest Chemistry analyzer (IDEXX Laboratories) according to the manufacturer's instructions.

FACS analysis

Cells were labeled with fluorescence tagged antibodies; using anti-mouse CD16/CD32 (mouse Fc blocker, Clone 2.4G2) (BD Pharmingen) and the Live/Dead fixable aqua dead cell stain kit with detection at 405 nm (Thermo Fisher Scientific). Infiltrating macrophages ($CD11b^+$, $F4/80^{low}$) and Kupffer cells ($CD11b^+$, $F4/80^{high}$) were gated using eFlour 450-conjugated anti-mouse CD45 (Clone 30-F11), PE-F4/80 (Clone BM8) (eBioscience), anti-mouse APC, APC-Cy7, or V500-CD11b (Clone M1/70) (BD Pharmingen), as well as with anti-mouse FITC, PerCP-Cy5.5 or APC-Cy7-Ly-6C (Clone AL-21) and anti-mouse APC or PE-CCR2 (Clone #475301) (R&D Systems). LSECs ($CD11b^-$, $CD146^+$) were also analyzed using eFlour 450-conjugated anti-mouse CD45 (Clone 30-F11) and anti-mouse PE-CD146 (Clone ME-9F1) (BD Pharmingen). Cells were read with FACS LSRII (BD Biosciences), and data were analyzed with FlowJo software (FlowJo LLC).

Calculation of shear stress

To evaluate hepatic hemodynamics and relevant functions of LSECs, the flow rate was adjusted as described (Ballermann

et al., 1998), with the estimated shear stress calculated as:

$$\tau = \frac{4\eta Q}{\pi R^3}$$

where τ = shear stress (dyn/cm^2); η = viscosity (dyne·sec/cm^2); Q = fluid flow rate (ml/sec); R = internal radius (cm).

In this system, the viscosity of the cell culture medium containing 10% FBS was approximately 0.008 dyne·sec/cm^2 and the internal radius of the inserted catheter was 0.09 cm. As the mouse portal vein has an internal radius of about 0.12 cm and a physiological blood flow rate of 1.6-2.3 ml/min (Xie et al., 2014), the flow rate of 1 ml/min in this system provides a shear stress similar to the actual physiologic shear stress. In our system, the roller pump speed of 6 rpm was well corresponded to 1 ml/min. The optimal pump speed should be set individually for each laboratory condition to 1 ml/min. To assess shear stress-induced LSEC stimulation, the flow rate was increased to 3 ml/min.

Statistical analysis

All statistical analyses were performed using Prism version 7.0 (GraphPad Software). Data are presented as the mean ± sem. Differences between two groups were evaluated using unpaired Student's *t* tests, with a *P* value <0.05 considered statistically significant.

RESULTS

In situ liver perfusion maintains cell viability and metabolic function

To show that the circulation of culture medium maintains liver cell viability and related metabolic functions, mice were sacrificed and left for 2 h with or without *in situ* liver perfusion. While the parenchyma was dissolved and the hepatocytes were singularized in the control group, the structure of the liver parenchyma remained relatively intact in the mice that underwent *in situ* liver perfusion even compared to the fresh liver (Fig. 3A). Moreover, cell viability, as assessed by TUNEL staining, was significantly higher in mice that underwent *in situ* liver perfusion than in control mice (Figs. 3A and 3B). Hepatic function, as determined by the levels of expression of genes encoding albumin, CYP2E1, and glucose-6-

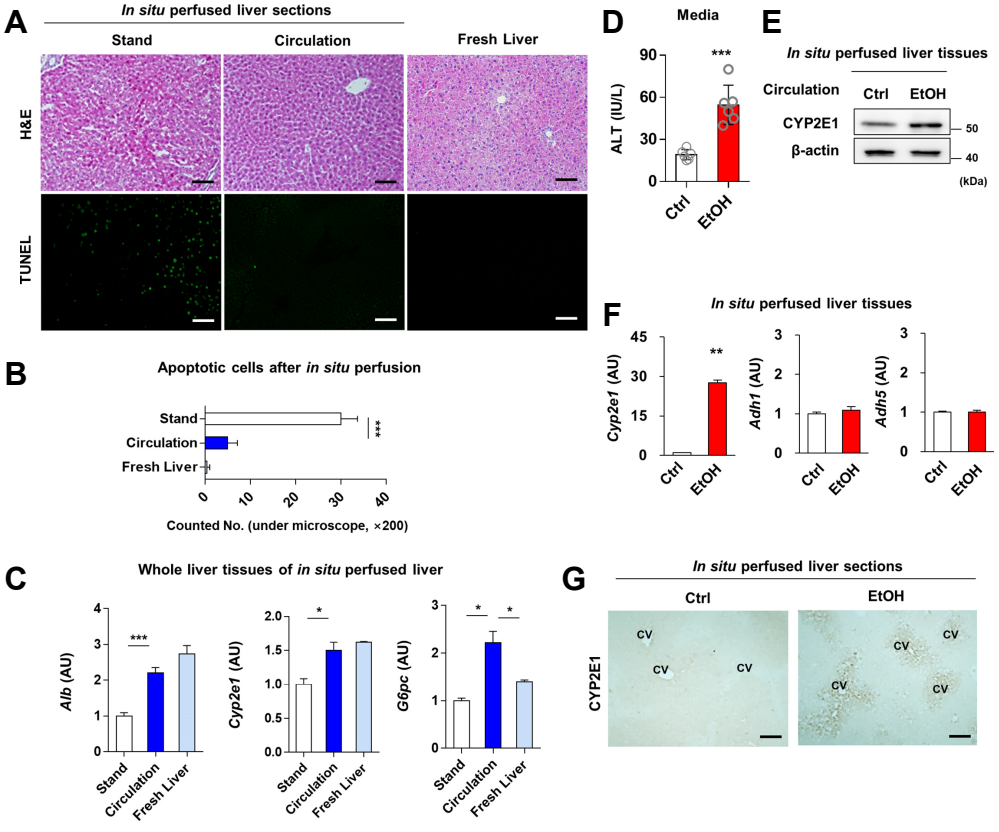

Fig. 3. *In situ* liver perfusion maintains cell viability and function. (A-C) Mice were sacrificed and perfused *in situ* with DMEM containing 10% FBS and 1% penicillin-streptomycin or not perfused. (A) Representative H&E and TUNEL staining. Scale bars = 50 μm. (B) Numbers of apoptotic cells assessed by TUNEL staining. (C) Levels of hepatic *Alb*, *Cyp2e1*, and *G6pc* mRNAs. (D-G) Mouse livers were perfused *in situ* with medium with (EtOH) or without (Ctrl) 100 mM ethanol for 2 h. (D) ALT levels in the medium. (E) Immunoblot assays for CYP2E1. Full-length blots are presented in Supplementary Fig. S2. (F) qRT-PCR assays for *Cyp2e1*, *Adh1*, and *Adh5*. (G) Representative CYP2E1 immunohistochemical staining. Scale bars = 50 μm. Gene expression was normalized relative to that of *Actb*. Data are shown as mean ± sem. $*P < 0.05$, $**P < 0.01$, $***P < 0.001$ versus the corresponding control.

phosphatase, was also significantly higher in the mice that underwent *in situ* liver perfusion (Fig. 3C). Moreover, the gene expressions of albumin and CYP2E1 from the liver of mice after *in situ* perfusion was also comparable to those from the fresh liver (Fig. 3C). The gene expression of *G6pc* encoding glucose-6-phosphatase was even higher in the liver of mice with *in situ* perfusion than the fresh liver (Fig. 3C), probably due to high glucose content (4.5 g/l) in circulating medium which paradoxically increases *G6pc* gene expression as shown in the previous studies (Gautier-Stein et al., 2012; Massillon et al., 1996).

The hepatocellular function and viability remained nearly stable during the perfusion period up to 2 h; however, the function and viability were remarkably decreased after 2 h of *in situ* liver perfusion as assessed by the gene expressions of albumin and CYP2E1 and TUNEL staining, respectively (Supplementary Fig. S1). Increased hypoxic stress is presumed to be responsible for tissue damage and increased apoptosis, indicated by elevated LDH in circulated medium and HIF-1α and cleaved caspase 3 expressions in the liver after 2 h of *in situ* liver perfusion (Lee et al., 2018)(Supplementary Fig. S1).

To assess the actual effects of *in situ* liver perfusion on metabolism and toxicology, mice were perfused for 2 h with medium that did or did not contain 100 mM ethanol. Acute liver injury, as indicated by the elevation of ALT (Fig. 3D), was observed following perfusion with medium containing ethanol. In addition, *in situ* liver perfusion with ethanol increased the expression of CYP2E1 protein (Fig. 3E), which induces alcoholic liver injury (Lu et al., 2008). However, there were no differences in the expression of genes encoding other alcohol metabolizing enzymes such as *Adh1* and *Adh5* (Fig. 3F). Immunohistochemical staining also showed that perfusion with medium containing ethanol induced the expression of CYP2E1 around the central vein (Fig. 3G), an indicator of the pathology of *in vivo* mouse models of alcoholic liver injury and of alcoholic patients. Collectively, these results suggested that *in situ* liver perfusion with ethanol for 2 h was sufficient to induce CYP2E1 activity and promote acute alcoholic liver injury.

In situ liver perfusion with a particular ligand is suitable to evaluate the downstream pathway in the liver

To investigate whether *in situ* liver perfusion can assess the downstream effect of particular ligands, mouse livers were perfused *in situ* with medium containing various ligands, such as IFN-γ and polyinosinic-polycytidylic acid (poly I:C) (Fig. 4A). IFN-γ binding to its receptor leads to the downstream tyrosine phosphorylation of STAT1; with STAT1 homodimers translocating into the nucleus and binding to IFN-γ-activated sites (GAS), thereby inducing the expression of IFN-γ target genes (Aaronson and Horvath, 2002). Immunoblotting of liver tissues after *in situ* liver perfusion with IFN-γ showed significant increases in phosphorylated STAT1 (Fig. 4B) and the expression of IFN-γ target genes, such as *Irf1*, *Socs1*, and *Nos2* (Fig. 4C).

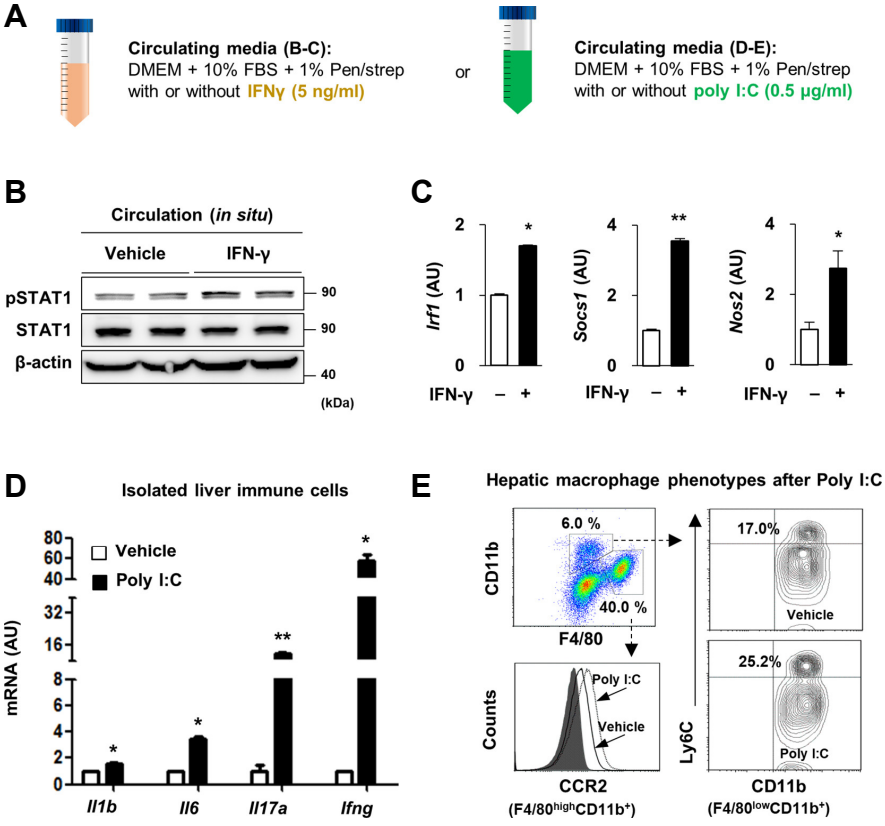

Fig. 4. *In situ* liver perfusion with ligand activates the downstream pathway in the liver. (A) Schematic figure of the experiments. (B-C) *In situ* liver perfusion with medium with or without IFN-γ (5 ng/ml) for 1 h. (B) Immunoblot assays for pSTAT1 and STAT1. Full-length blots are presented in Supplementary Fig. S3. (C) Expression of *Irf1*, *Socs1*, and *Nos2* mRNAs in whole liver tissues. (D-E) *In situ* liver perfusion with medium with or without poly I:C (0.5 μg/ml) for 1 h. (D) Expression of *Il1b*, *Il6*, *Il17a*, and *Ifng* mRNAs by isolated hepatic immune cells. (E) Flow cytometric analyses of isolated hepatic immune cells. Gene expression was normalized relative to that of *Actb*. Data are shown as mean ± sem. $*P < 0.05$, $**P < 0.01$ versus the corresponding control.

Poly I:C is structurally similar to double-stranded RNA, which can activate toll-like receptor 3 in various types of immune cells (Seo et al., 2016). Perfusion with medium containing poly I:C significantly increased the expression of genes encoding pro-inflammatory cytokines, such as *Il1b*, *Il6*, *Il17a*, and *Ifng*, in hepatic immune cells (Fig. 4D). Moreover, perfusion with poly I:C increased the expression of C-C chemokine receptor type 2 (CCR2) in Kupffer cells ($CD11b^{+}$, $F4/80^{high}$) and the percentage of $Ly6C^{+}$ cells among infiltrated macrophages ($CD11b^{+}$, $F4/80^{low}$) (Fig. 4E), suggesting that these immune cell subsets are activated by poly I:C.

Immune cell function can be evaluated by *in situ* liver perfusion

In vivo adoptive transfer through the tail vein has limitations in evaluating the migration to the liver of immune cells, especially minor subsets of immune cells, due to wide tissue distribution resulting from systemic injection. This limitation may be overcome by *in situ* liver perfusion, because the circulation of immune cells is restricted to the liver. In previous studies, we successfully adapted the *in situ* liver perfusion machinery to investigate the migration of Tregs (Lee et al., 2015; 2016), as well as the migration of γδ T cells following carbon tetrachloride (CCl_4)-mediated liver injury (Seo et al., 2016). In addition to assessing immune cell migration, *in situ* liver perfusion can evaluate immune cell function. Splenic lymphocytes were isolated from wild type mice and placed in circulating medium with or without concanavalin A (Con A) (Fig. 5A), which is widely used to study T cell-mediated hepatitis (Tiegs et al., 1992). Following *in situ* liver perfusion for 2 h, the expression of pro-inflammatory cytokines such as *Ifng* and *Il6* was markedly higher in the Con A-infused splenic lymphocytes than in those non-infused with Con A (Fig. 5B), resulting in increased STAT1 activity in the liver (Fig. 5C). Consistent with these findings, the expression of *Tnf* and of *Ccl2*, a chemokine that recruits monocytes, T cells and dendritic cells (Carr et al., 1994), was significantly higher in the presence than in the absence of Con A (Fig. 5D). As a result, hepatic damage, as indicated by ALT concentration and apoptotic cell death, was greater in Con A-treated than in control livers (Figs. 5E-5G).

In situ liver perfusion machinery can regulate shear stress to stimulate LSECs

One of the great advantages of this method of *in situ* liver perfusion machinery was the ability to evaluate hemodynamic change related reactions of LSECs. Mouse portal veins are approximately 1.2 mm in diameter and have a physiological blood flow rate of 1.6-2.3 ml/min (Xie et al., 2014). If other variables are identical, shear stress is proportional to fluid flow rate (Fig. 6A). Thus, shear stress to the liver during *in situ* liver perfusion can be adjusted by controlling its flow rate, with the relationship between estimated shear stress and flow rate being derived from the formula by which shear stress is based on the diameter and branch number of the portal vein (Figs. 6A and 6B). In general, leukocyte recruitment is followed by a multistep adhesion cascade, including chemokine-mediated chemotaxis (Ley et al., 2007). In the liver, most leukocyte recruitment occurs within the low shear hepatic sinusoids, which are lined by a unique population of LSECs. These cells are separated from hepatocytes by the space of Disse and are the first cells to contact circulating leukocytes. These LSECs express various chemokines and adhesion molecules; thereby playing a critical role in maintaining immune homeostasis in both physiologic and pathologic conditions (Shetty et al., 2018). Shear stress-induced monocyte chemoattractant protein-1 (MCP-1; also known as C-C motif chemokine ligand 2, CCL2) has been

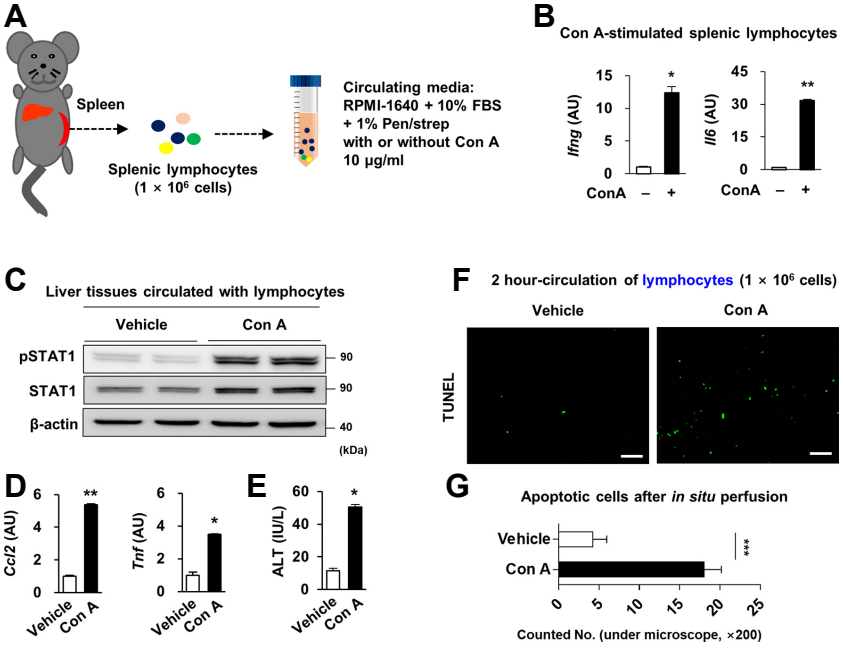

Fig. 5. *In situ* liver perfusion with Con A-induced activated lymphocytes damages the liver. (A-F) Splenic lymphocytes were isolated by grinding and placed in circulating medium with or without 10 μg/ml Con A, followed by in situ liver perfusion for 1 h. (A) Schematic figure of the experiment. (B) Expression of *Ifng* and *Il6* mRNAs by isolated splenic lymphocytes. (C) Immunoblot assays for pSTAT1 and STAT1 in whole liver tissues after perfusion. Full-length blots are presented in Supplementary Fig. S4. (D) Expression of *Ccl2* and *Tnf* mRNAs by whole liver tissues after perfusion. (E) ALT levels in circulating medium. (F) Representative TUNEL staining after perfusion. Scale bars = 50 μm. (G) Numbers of apoptotic cells assessed by TUNEL staining. Gene expression was normalized relative to that of *Actb*. Data are shown as mean ± sem. $*P < 0.05$, $**P < 0.01$, $***P < 0.001$ versus the corresponding control.

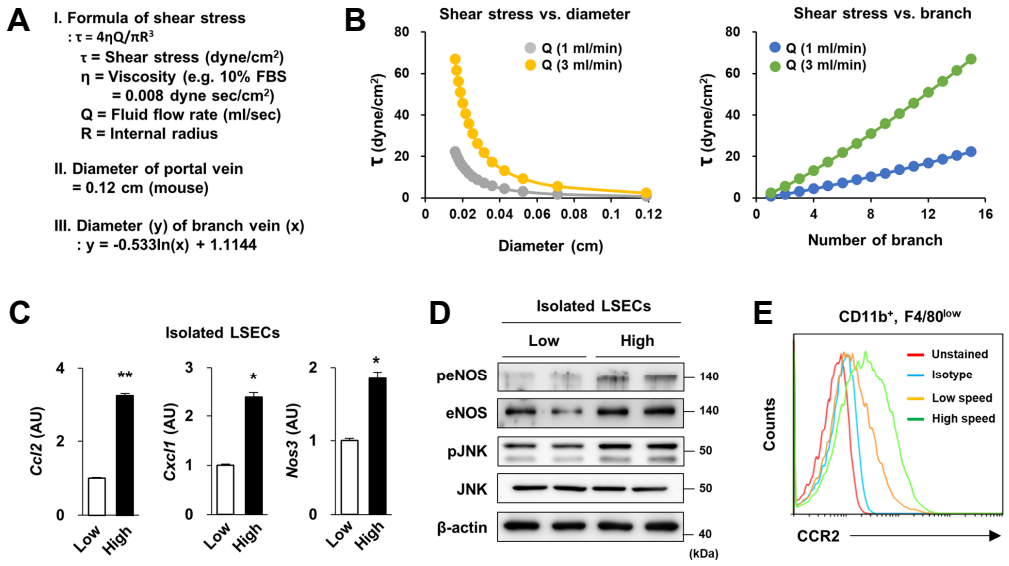

Fig. 6. Stimulation of liver sinusoidal endothelial cells (LSECs) by *in situ* liver perfusion-induced shear stress. Livers were perfused *in situ* with medium at flow rates of 1 ml/min (low) and 3 ml/min (high). (A-B) Formula for calculating shear stress and its dependence on vessel diameter and vessel branch number. (C) Expression of *Ccl2*, *Cxcl1*, and *Nos3* mRNAs by isolated LSECs. (D) Immunoblot analysis of peNOS, eNOS, pJNK and JNK by isolated LSECs. Full-length blots are presented in Supplementary Fig. S5. (E) FACS assessment of CCR2 expression in isolated $CD11b^{+}F4/80^{low}$ infiltrated monocytes. Data are presented as mean ± sem. $*P<0.05$, $**P<0.01$ versus the corresponding control.

shown to play a critical role in the pathogenesis of atherosclerosis by recruiting $CCR2^{+}$ monocytes to the vascular wall (Gu et al., 1998; Maus et al., 2002). In particular, shear stress-induced MCP-1 expression in endothelial cells is mediated through activator protein-1 (AP-1), which is phosphorylated through activation of the JNK pathway (Azuma et al., 2000; Braddock et al., 1998). To assess this phenomenon in the liver, livers were perfused *in situ* for 2 h at low (1 ml/min) and high (3 ml/min) circulation rates. Then, LSECs were isolated and subsequently purified by MACS, which yielded a purity >90 % (data not shown). As expected, the expression of genes encoding *Ccl2*, *Cxcl1*, and endothelial nitric oxide synthase (*Nos3*) were significantly higher in LSECs following circulation at 3 ml/min than at 1 ml/min (Fig. 6C), a finding paralleled by the activation of endothelial nitric oxide synthase and the JNK pathway (Fig. 6D). In addition, infiltrated monocytes ($CD11b^{+}$, $F4/80^{low}$ cells) exhibited higher expression of CCR2, the receptor for CCL2 at the higher rate of circulation than at the low rate of circulation (Fig. 6E). Collectively, these findings suggest that *in situ* liver perfusion provides a feasible model for studying mechanical stress-induced functional changes and activation of LSECs.

DISCUSSION

Various methods are currently used to study liver diseases, including the isolation and culture of primary cells, the precision-cut liver slice model, and the organoid model. As depicted in Fig. 1, isolating technique of rat hepatocytes was first developed in 1969 by Berry and Friend (Berry and Friend, 1969), and then further modified by Seglen (Seglen, 1976). Later in 1976, the isolation of human hepatocytes was introduced by Bojar (Bojar et al., 1976). At present, isolation of non-parenchymal cells as well as hepatocytes using differential and gradient centrifugation is widely used both in human and mouse (Mohar et al., 2015; Werner et al., 2015). These conventional *in vitro* primary cell culture models are useful in studying the intracellular pathways of each cell type, with co-culture of different cell types being useful in studying intercellular crosstalk. These approaches, however, have important drawbacks in modeling actual *in vivo* cellular events. For example, isolated cells lose their anatomical polarity and natural matrix, altering their original characteristics. Moreover, these approaches are unable to reproduce the complex *in vivo* environments of these cells. Immortalized cell lines derived from human (HepG2, Hep-3B, etc.) and mouse (Hepa 1-6, Hepa-1c1c7, etc.) livers are also available. Although these cell lines have some advantages over primary cells, in that they are easy to obtain and maintain, they express lower levels of metabolizing enzymes and their intrinsic characteristics differ from those of primary cell cultures.

The precision-cut liver slice model was developed to overcome the drawbacks of conventional cell culture models (De Graaf et al., 2010). In this method, fresh slices of liver tissues, including from mice and humans, are cut reproducibly and cultured. Although this model can mimic the actual *in vivo* environment as much as possible, it also has key drawbacks. For example, it requires special equipment such as a tissue slicer, and it does not allow full penetration of compounds under some conditions, particularly lipophilic compounds that are rapidly metabolized by the outer cell layers of these slices (Worboys et al., 1997). Moreover, this method does

not allow for the study of the role of hepatic immune cells or hepatic hemodynamics.

Another novel technique is organoid culture, which enables the long-term expansion and genetic manipulation of adult livers in 3D culture systems (Broutier et al., 2016). Organoid cultures provide an extracellular matrix environment, along with a mixture of growth factors that are vital during liver development and regeneration (such as HGF, EGF, FGF, and R-spondin-1) (Duncan et al., 2009; Huch et al., 2013; Zaret and Grompe, 2008). A recent study provided a detailed protocol for growing adult mouse and human liver organoids, from cell isolation and long-term expansion to genetic manipulation *in vitro* (Broutier et al., 2016). This technique provides an opportunity to create cellular models of human diseases. Furthermore, organoid culture can easily be manipulated genetically, using retroviruses or CRISPR/Cas endonuclease systems. However, this culture system also has limitations, including the long time (1-4 weeks) required to generate organoids. Moreover, although liver buds derived from hiPSCs and co-cultured with mesenchymal and endothelial cells generated liver buds containing both mesenchymal and epithelial cells (Wang et al., 2014), most of these cultures result only in the expansion of the adult epithelial compartment. In addition, these cultures are limited in interactions with immune cells and in assessing hepatic hemodynamics and the stem-cell niche, limiting their ability to assess actual *in vivo* environments. Thus, despite the advantages of organoid culture model, a new methodology was required to compensate for these limitations.

This study describes a protocol for *in situ* perfusion of mouse livers. The method is very simple and can be used to complement rather than replace the above-described methods in a variety of applications. The *in situ* liver perfusion method, originally called the isolated perfused rat liver (IPRL) model, was developed initially in rats (Gores et al., 1986) and, after some modifications, widely used to investigate the physiology and pathophysiology of the rat liver. The IPRL model has been used to investigate ischemia-reperfusion injury; the metabolism of compounds, ammonium, and amino acids (Häussinger, 1987), protein synthesis (Lindell et al., 1994; Tavill, 1972), oxygen consumption (Dahn et al., 1999), and LSEC function using hyaluronic acid uptake (Reinders et al., 1996). This model is useful in evaluating specific aspects of liver function *in situ* in the absence of systemic effects (Gores et al., 1986; Tygstrup, 1975).

As the use of mice rather than rats has many advantages, including lower maintenance costs and the availability of a wide range of genetic models, the rat model in studying liver disease has shifted largely to the mouse model in recent years. In keeping with this trend, *in situ* liver perfusion machinery has subsequently been adapted to mice in our laboratory. In addition, mouse livers are smaller in size than rat livers, resulting in better oxygenation of the liver parenchyma in the former. In previous studies from our laboratory, we adapted the isolated liver perfusion model in mice to various experimental conditions, allowing investigations of the migration of Tregs (Lee et al., 2015; 2016), the migration of γδ T cells in CCl_4-mediated injured livers (Seo et al., 2016), and the palmitate-induced generation of reactive oxygen species in immune cells of the livers of various knockout mice (Kim et al., 2017). This study expands the applications of this method, showing that *in situ* liver perfusion can be used to assess the metabolism of toxic materials such as ethanol, the direct effects of various ligands on the liver, immune cell function, and shear stress-induced LSEC stimulation.

One of the critical drawbacks of the *in situ* liver perfusion method is the insufficient oxygenation of the liver parenchyma. This may be circumvented by increasing the infusate flow rate, enhancing oxygen supply to the parenchyma. However, increased flow rate may induce shear-stress-induced injury to LSECs. Alternatively, an oxygenator can be applied to increase dissolved oxygen concentration in the circulating media; or oxygen carriers such as perfluorcarbons or erythrocytes can be added to the circulating media to aid oxygen transfer to the liver parenchyma during perfusion (Bessems et al., 2006). Another drawback is the maximum circulation time, which is only 2 h. At longer times, cell viability and function dramatically deteriorate (Supplementary Fig. S1). This limitation must be considered when analyzing long-term rather than immediate-early responses of the liver. Considering this point, it may be more useful to apply *in situ* liver perfusion method to see the liver-specific response secondarily after disease development in mice such as CCl_4-induced liver fibrosis or high fat diet-induced nonalcoholic fatty liver disease. Further research is required to increase the total circulating time. Although one of the advantages of the *in situ* liver perfusion method is the ability to evaluate liver-specific responses, by excluding the effect of other organs, in other words, various interorgan interactions that occur *in vivo* cannot be assessed.

This *in situ* liver perfusion method may provide a simple but widely applicable method. *In situ* liver perfusion can be performed sequentially after *in vivo* disease modeling, such as CCl_4-induced liver fibrosis or high fat diet-induced nonalcoholic fatty liver disease. Moreover, *in situ* liver perfusion may provide a greater understanding of the mechanism of liver diseases by isolating each cell type and exploring its cellular reactions. This *in situ* liver perfusion machinery may therefore provide a more comprehensive understanding of liver pathogenesis and the mechanistic pathways in liver diseases.

Note: Supplementary information is available on the Molecules and Cells website (www.molcells.org).

ACKNOWLEDGMENTS

This work was supported by grants from the National Research Foundation of Korea (NRF) funded by the Korea government (MSIT) (2015R1A2A1A10055551, 2018R1C1B6004439), the Korea Mouse Phenotyping Project (2014M3A9D5A01073556) of the National Research Foundation funded by the Ministry of Science & ICT, the Intelligent Synthetic Biology Center of Global Frontier Project funded by the Ministry of Science, ICT & Future Planning (2011-0031955) Republic of Korea.

REFERENCES

Aaronson, D.S., and Horvath, C.M. (2002). A road map for those

who don't know JAK-STAT. Science *296*, 1653-1655.

Azuma, N., Duzgun, S.A., Ikeda, M., Kito, H., Akasaka, N., Sasajima, T., and Sumpio, B.E. (2000). Endothelial cell response to different mechanical forces. J. Vasc. Surg. *32*, 789-794.

Ballermann, B.J., Dardik, A., Eng, E., and Liu, A. (1998). Shear stress and the endothelium. Kidney Int. Suppl. *54*, S100-S108.

Berry, M., and Friend, D. (1969). High-yield preparation of isolated rat liver parenchymal cells: a biochemical and fine structural study. J. Cell. Biol. *43*, 506-520.

Bessems, M., 't Hart, N., Tolba, R., Doorschodt, B., Leuvenink, H., Ploeg, R., Minor, T., and Van Gulik, T. (2006). The isolated perfused rat liver: standardization of a time-honoured model. Lab. Anim. *40*, 236-246.

Blouin, A., Bolender, R.P., and Weibel, E.R. (1977). Distribution of organelles and membranes between hepatocytes and nonhepatocytes in the rat liver parenchyma. A stereological study. J. Cell. Biol. *72*, 441-455.

Bojar, H., Basler, M., Fuchs, F., Dreyfürst, R., Staib, W., and Broelsch, C. (1976). Preparation of parenchymal and non-parenchymal cells from adult human liver—morphological and biochemical characteristics. J. Clin. Chem. Clin. Biochem. *14*, 527-532.

Braddock, M., Schwachtgen, J.-L., Houston, P., Dickson, M.C., Lee, M.J., and Campbell, C.J. (1998). Fluid shear stress modulation of gene expression in endothelial cells. News. Physiol. Sci. *13*, 241-246.

Broutier, L., Andersson-Rolf, A., Hindley, C.J., Boj, S.F., Clevers, H., Koo, B.-K., and Huch, M. (2016). Culture and establishment of self-renewing human and mouse adult liver and pancreas 3D organoids and their genetic manipulation. Nat. Protoc. *11*, 1724-1743.

Carr, M.W., Roth, S.J., Luther, E., Rose, S.S., and Springer, T.A. (1994). Monocyte chemoattractant protein 1 acts as a T-lymphocyte chemoattractant. Proc. Natl. Acad. Sci. USA *91*, 3652-3656.

Dahn, M.S., Lange, M.P., and Benn, S. (1999). The influence of hepatic venous oxygen saturation on the liver's synthetic response to metabolic stress. Proc. Soc. Exp. Biol. Med. *221*, 39-45.

De Graaf, I.A., Olinga, P., De Jager, M.H., Merema, M.T., De Kanter, R., Van De Kerkhof, E.G., and Groothuis, G.M. (2010). Preparation and incubation of precision-cut liver and intestinal slices for application in drug metabolism and toxicity studies. Nat. Protoc. *5*, 1540-1551.

Duncan, A.W., Dorrell, C., and Grompe, M. (2009). Stem cells and liver regeneration. Gastroenterol. *137*, 466-481.

Gao, B., Jeong, W.I., and Tian, Z. (2008). Liver: an organ with predominant innate immunity. Hepatol. *47*, 729-736.

Gautier-Stein, A., Soty, M., Chilloux, J., Zitoun, C., Rajas, F., and Mithieux, G. (2012). Glucotoxicity induces glucose-6-phosphatase catalytic unit expression by acting on the interaction of HIF-1α with CREB-binding protein. Diabetes *61*, 2451-2460.

Gores, G.J., Kost, L.J., and Larusso, N.F. (1986). The isolated perfused rat liver: conceptual and practical considerations. Hepatol. *6*, 511-517.

Gu, L., Okada, Y., Clinton, S.K., Gerard, C., Sukhova, G.K., Libby, P., and Rollins, B.J. (1998). Absence of monocyte chemoattractant protein-1 reduces atherosclerosis in low density lipoprotein receptor-deficient mice. Mol. Cell *2*, 275-281.

Häussinger, D. (1987). Isolated perfused rat liver: an experimental model for studies on ammonium and amino acid metabolism. Transfus. Med. Hemother. *14*, 174-178.

Huch, M., Dorrell, C., Boj, S.F., Van Es, J.H., Li, V.S., Van De Wetering, M., Sato, T., Hamer, K., Sasaki, N., Finegold, M.J., et al. (2013). *In vitro* expansion of single Lgr5^{+} liver stem cells induced by Wnt-driven regeneration. Nature *494*, 247-250.

Kim, S.Y., Jeong, J.-M., Kim, S.J., Seo, W., Kim, M.-H., Choi, W.-M., Yoo, W., Lee, J.-H., Shim, Y.-R., Yi, H.-S., et al. (2017). Pro-inflammatory hepatic macrophages generate ROS through NADPH oxidase 2 via endocytosis of monomeric TLR4-MD2 complex. Nat. Commun. *8*, 2247.

Lee, Y.S., Yi, H.S., Suh, Y.G., Byun, J.S., Eun, H.S., Kim, S.Y., Seo, W., Jeong, J.M., Choi, W.M., Kim, M.H., et al. (2015). Blockade of retinol metabolism protects T cell-induced hepatitis by increasing migration of regulatory T cells. Mol. Cells *38*, 998-1006.

Lee, Y.S., Eun, H.S., Kim, S.Y., Jeong, J.M., Seo, W., Byun, J.S., Jeong, W.I., and Yi, H.S. (2016). Hepatic immunophenotyping for streptozotocin-induced hyperglycemia in mice. Sci. Rep. *6*, 30656.

Lee, Y.S., Park, K.M., Yu, L., Kwak, H.H., Na, H.J., Kang, K.S., and Woo, H.M. (2018). Necroptosis is a mechanism of death in mouse induced hepatocyte-like cells reprogrammed from mouse embryonic fibroblasts. Mol. Cells *41*, 639-645.

Ley, K., Laudanna, C., Cybulsky, M.I., and Nourshargh, S. (2007). Getting to the site of inflammation: the leukocyte adhesion cascade updated. Nat. Rev. Immunol. *7*, 678-689.

Lindell, S.L., Southard, J.H., Vreugdenhil, P., and Belzer, F.O. (1994). Kupffer cells depress hepatocyte protein synthesis on cold storage of the rat liver. Transplantation *58*, 869-874.

Lu, Y., Zhuge, J., Wang, X., Bai, J., and Cederbaum, A.I. (2008). Cytochrome P450 2E1 contributes to ethanol-induced fatty liver in mice. Hepatol. *47*, 1483-1494.

Massillon, D., Barzilai, N., Chen, W., Hu, M., and Rossetti, L. (1996). Glucose regulates in vivo glucose-6-phosphatase gene expression in the liver of diabetic rats. J. Biol. Chem. *271*, 9871-9874.

Maus, U., Henning, S., Wenschuh, H., Mayer, K., Seeger, W., and Lohmeyer, J. (2002). Role of endothelial MCP-1 in monocyte adhesion to inflamed human endothelium under physiological flow. Am. J. Physiol. Heart. Circ. Physiol. *283*, H2584-H2591.

Mederacke, I., Dapito, D.H., Affò, S., Uchinami, H., and Schwabe, R.F. (2015). High-yield and high-purity isolation of hepatic stellate cells from normal and fibrotic mouse livers. Nat. Protoc. *10*, 305-315.

Mohar, I., Brempelis, K.J., Murray, S.A., Ebrahimkhani, M.R., and Crispe, I.N. (2015). Isolation of non-parenchymal cells from the mouse liver. Methods. Mol. Biol. *1325*, 3-17.

Reinders, M.E., Wagensveld, B.A., Gulik, T.M., Frederiks, W.M., Chamuleau, R.A., Endert, E., and Klopper, P.J. (1996). Hyaluronic acid uptake in the assessment of sinusoidal endothelial cell damage after cold storage and normothermic reperfusion of rat livers. Transpl. Int. *9*, 446-453.

Seglen, P.O. (1976). Preparation of isolated rat liver cells. Methods. Cell. Biol. *13*, 29-83.

Seo, W., Eun, H.S., Kim, S.Y., Yi, H.S., Lee, Y.S., Park, S.H., Jang, M.J., Jo, E., Kim, S.C., Han, Y.M., et al. (2016). Exosome-mediated activation of toll-like receptor 3 in stellate cells stimulates interleukin-17 production by γδ T cells in liver fibrosis. Hepatol. *64*, 616-631.

Shetty, S., Lalor, P.F., and Adams, D.H. (2018). Liver sinusoidal endothelial cells—gatekeepers of hepatic immunity. Nat. Rev. Gastroenterol. Hepatol. *15*, 555-567.

Tavill, A. (1972). The synthesis and degradation of liver-produced proteins. Gut. *13*, 225-241.

Tiegs, G., Hentschel, J., and Wendel, A. (1992). AT cell-dependent experimental liver injury in mice inducible by concanavalin A. J. Clin. Invest. *90*, 196-203.

Tygstrup, N. (1975). Aspects of hepatic hypoxia: observations on the

isolated, perfused pig liver. Bull. N. Y. Acad. Med. *51*, 551-556.

Wang, N., Zhang, H., Zhang, B.-Q., Liu, W., Zhang, Z., Qiao, M., Zhang, H., Deng, F., Wu, N., Chen, X., et al. (2014). Adenovirus-mediated efficient gene transfer into cultured three-dimensional organoids. PLoS. One *9*, e93608.

Werner, M., Driftmann, S., Kleinehr, K., Kaiser, G.M., Mathé, Z., Treckmann, J.-W., Paul, A., Skibbe, K., Timm, J., and Canbay, A., et al. (2015). All-in-one: advanced preparation of human parenchymal and non-parenchymal liver cells. PLoS. One *10*, e0138655.

Worboys, P.D., Bradbury, A., and Houston, J.B. (1997). Kinetics of drug metabolism in rat liver slices: III. Relationship between metabolic clearance and slice uptake rate. Drug. Metab. Dispos. *25*, 460-467.

Xie, C., Wei, W., Zhang, T., Dirsch, O., and Dahmen, U. (2014). Monitoring of systemic and hepatic hemodynamic parameters in mice. J. Vis. Exp. *4*, e51955.

Zaret, K.S., and Grompe, M. (2008) Generation and regeneration of cells of the liver and pancreas. Science *322*, 1490-1494.